

## Exploring the Photon-Number Distribution of Bimodal Microlasers with a Transition Edge Sensor

Elisabeth Schlottmann,<sup>1</sup> Martin von Helversen,<sup>1</sup> Heinrich A. M. Leymann,<sup>2,\*</sup> Thomas Lettau,<sup>3</sup> Felix Krüger,<sup>1</sup> Marco Schmidt,<sup>1,4</sup> Christian Schneider,<sup>5</sup> Martin Kamp,<sup>5</sup> Sven Höfling,<sup>5,6</sup> Jörn Beyer,<sup>4</sup> Jan Wiersig,<sup>3</sup> and Stephan Reitzenstein<sup>1,†</sup>

<sup>1</sup>*Institut für Festkörperphysik, Quantum Devices Group, Technische Universität Berlin, Hardenbergstraße 36, EW 5-3, 10623 Berlin, Germany*

<sup>2</sup>*Max-Planck-Institut für Physik komplexer Systeme, Nöthnitzer Straße 38, 01187 Dresden, Germany*

<sup>3</sup>*Institut für Theoretische Physik, Otto-von-Guericke-Universität Magdeburg, Universitätsplatz 2, 39106 Magdeburg, Germany*

<sup>4</sup>*Physikalisch-Technische Bundesanstalt, Abbestraße 2-12, 10587 Berlin, Germany*

<sup>5</sup>*Technische Physik, Universität Würzburg, Am Hubland, 97074 Würzburg, Germany*

<sup>6</sup>*SUPA, School of Physics and Astronomy, University of St Andrews, St Andrews KY16 9SS, United Kingdom*

 (Received 25 September 2017; revised manuscript received 11 April 2018; published 19 June 2018)

A photon-number-resolving transition edge sensor (TES) is used to measure the photon-number distribution of two microcavity lasers. The investigated devices are bimodal microlasers with similar emission intensity and photon statistics with respect to the photon autocorrelation. Both high- $\beta$  microlasers show partly thermal and partly coherent emission around the lasing threshold. For higher pump powers, the strong mode of microlaser *A* emits Poissonian distributed photons, while the emission of the weak mode is thermal. By contrast, laser *B* shows a bistability resulting in overlaid thermal and Poissonian distributions. While a standard Hanbury Brown and Twiss experiment cannot distinguish between the simple thermal emission of laser *A* and the temporal mode switching of the bistable laser *B*, TESs allow us to measure the photon-number distribution, which provides important insight into the underlying emission processes. Indeed, our experimental data and their theoretical description by a master equation approach show that TESs are capable of revealing subtle effects like the mode switching of bimodal microlasers. As such, we clearly demonstrate the benefit and importance of investigating nanophotonic devices via photon-number-resolving transition edge sensors.

DOI: [10.1103/PhysRevApplied.9.064030](https://doi.org/10.1103/PhysRevApplied.9.064030)

### I. INTRODUCTION

Analyzing the photon statistics using a Hanbury Brown and Twiss (HBT) configuration is a well-established method in quantum optics [1] which essentially measures the time correlation of photon pairs to determine the second-order autocorrelation function  $g^{(2)}(\tau)$ . However, a full understanding of the processes involved in the emission of such nanophotonic devices often requires not only the information quantified in  $g^{(2)}(0)$  but also knowledge of the photon-number distribution.

The challenge of determining the photon-number distribution of emission can be tackled by using photon-number-resolving detectors. Unfortunately, standard single-photon-sensitive detectors based on avalanche photodiodes

are not capable of measuring the number of impinging photons. This shortcoming is not present for another class of highly efficient detectors—namely, transition edge sensors (TESs; see Fig. 1). Such detectors usually have high quantum efficiency in excess of 90% over a large range of wavelengths [2] and can be used as photon-number-resolving detectors because of their calorimetric operation principle [3,4]. Interestingly, in spite of the advantage of being able to experimentally access the photon-number distribution of ultralow-light-level emitters [5], TESs have not yet been applied for an in-depth analysis of nanophotonic devices.

Knowledge about the photon-number distribution of nanophotonic devices allows one to better understand their operation and to improve their application in fields where nonlinear processes are dominant—e.g., for ghost imaging [6], subwavelength lithography [7], metrology [8], and two-photon-excited fluorescence [9,10]. Here, we investigate two bimodal microlasers and explore diverse characteristics in their full photon statistics. It is interesting to

\*Present address: INO-CNR BEC Center and Dipartimento di Fisica, Università di Trento, I-38123 Povo, Italy.

†stephan.reitzenstein@physik.tu-berlin.de

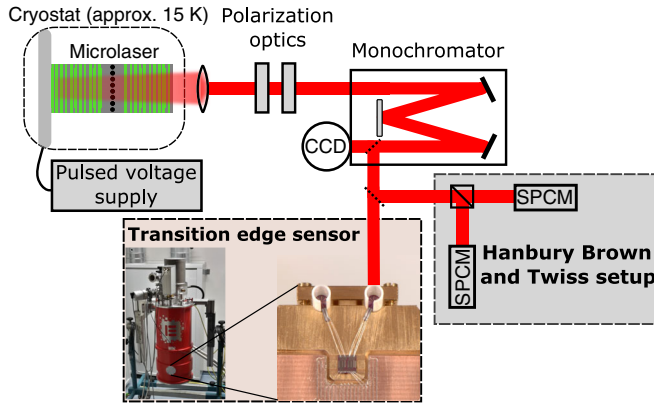


FIG. 1. Sketch of the experimental setup. The microlaser sample is operated in a He-flow cryostat at 15 K and is excited by a pulsed electrical voltage supply. The emitted light is analyzed by a spectrometer or the TES or, alternatively, by a standard HBT setup. SPCM denotes single-photon counting module.

note that, even though intensity fluctuations of two-mode (ring) lasers have been studied using photomultiplier tubes in photon-counting mode (see, e.g., Ref. [11]), these detectors are not able to determine the photon-number distribution of microlasers in the few-photon limit. By contrast, TES detectors are close-to-ideal devices to experimentally explore this distribution because of their high quantum efficiency and photon-number-resolving capabilities.

Microlasers are of strong interest for both fundamental research of cavity-enhanced nanophotonic devices and their future applications due to their small size, high speed, and low energy consumption [12]—for instance, in the field of quantum nanophotonics [13]. Popular microlaser concepts are based on photonic crystal cavities [14], plasmonic resonators [15], or micropillar cavities [16,17]. These resonator structures have small mode volumes in common, which result in enhanced light-matter coupling. Consequently, the associated spontaneous emission factor  $\beta$ , which is the fraction of spontaneously emitted light coupled into the cavity mode, is strongly enlarged so that the ultimate limit of thresholdless lasing can be approached [18].

In devices with high  $\beta$  factors, analyzing the input-output characteristics is not sufficient to prove lasing operation due to the lack of a significant nonlinearity at the threshold [19]. Furthermore, optical injection, superradiance, mode competition, and saturation of the low-dimensional gain medium can also lead to deviations from the standard behavior [20–25].

Studying the correlation of photon pairs has become an important tool to characterize microlasers, as it reveals the transition from predominantly spontaneous emission towards stimulated emission at threshold by a change of  $g^{(2)}(0)$  from 2 to 1 [26]. Interestingly, in bimodal lasers, additional effects like gain competition [22,27] and dissipative coupling [28] occur which are difficult to identify using a HBT measurement alone.

In this article, we apply a TES to measure the photon-number distribution of two microlasers with two orthogonally polarized modes. The TES allows us to obtain deeper insight into the emission properties, which is hardly possible using standard characterization tools such as a HBT configuration. Our work also highlights the big potential of TESs as an important measurement concept in the application of microlasers and in the wide field of nanophotonics. To illustrate this potential, we select two bimodal microlasers with, at first sight, very similar emission features. For the first laser, *A*, the emission of both modes is in a transient state from thermal to coherent light around the laser threshold. While for high pump rates the stronger mode emits pure coherent light, the weaker mode is in the thermal regime. The second laser, *B*, has similar input-output characteristics and  $g^{(2)}(0)$  values. Excitingly, for this laser gain competition between the two emission modes leads to mode bistability and an associated double-peaked photon-number distribution. The latter can be revealed only with the TES technique and is best described by an overlay of thermal and Poissonian statistics.

## II. THEORETICAL METHODS

To calculate the full photon statistics  $P_n$  of emission from the microlaser, we solve a master equation for the diagonal elements of the density matrix  $\rho_N^n$  giving the probabilities of finding the system in a state with photon numbers  $\mathbf{n} = (n_w, n_s)$  in the weak and in the strong mode of the laser and  $N$  excited emitters. The master equation is a multimode generalization of the equation used in Ref. [21] and is based on a statistical birth-death model including all relevant processes of a multimode laser on a phenomenological level.

Classical ring lasers in particular [29], but also microlasers based on photonic crystals [30] and micropillars [27], have been modeled with Langevin equations where the spontaneous emission is introduced by a random force or by Fokker-Planck equations for the (quasi)probability distribution of the electric field [29,31,32]. Within our model, we follow the quantum-mechanical approach introduced in Ref. [21], which is based on Ref. [33] and which gives a statistical representation of the Einstein rate equations for the photon probability distribution. It thus includes spontaneous emission and the discrete nature of the distribution.

The mean-field equations for the field intensities derived from our model are identical with the two-level-emitter limiting case of the microscopic laser theory developed in Ref. [34]. This model has been applied successfully to bimodal microcavity lasers before, to address the origin of superthermal intensity fluctuations [22] and to investigate the connection between nonequilibrium Bose-Einstein condensation [35] and pump-power-driven switching of the lasing mode in Ref. [36]. We take the finite coherence time of the signal and the finite temporal resolution of the

detector into account by folding the  $g^{(2)}(\tau)$  signal with the detector function [26].

As reported in Ref. [37], the nonlasing weak mode also has a relatively large coherence time for high pump rates. Thus, we can detect the super-Poissonian  $g^{(2)}(0)$  in this region, in contrast to the situation below the threshold pump rate, where the low coherence time hinders its detection. To describe the detection of photons emitted by the microlaser with the TES, a detection model introduced in Ref. [38] is used. The pulsed excitation and detection applied in this work is theoretically described by two steps: First, the steady state of the laser system is found for a pump rate corresponding to the pump area. Second, this steady state decays via the leaky cavity and the leaked and detected photons are counted (for further details, see the Appendix).

### III. SAMPLE TECHNOLOGY AND EXPERIMENTAL SETUP

The gain medium of the microlasers used is composed of a single layer of  $\text{In}_{0.3}\text{Ga}_{0.7}\text{As}$  quantum dots with a density of  $5 \times 10^9/\text{cm}^2$ . The active layer is embedded in the central  $1\text{-}\lambda$  GaAs cavity, which is sandwiched between an upper (lower) distributed Bragg reflector consisting of 26 (30) mirror pairs that are based on  $\lambda/4$ -thick layers of GaAs and AlAs. Micropillars of  $4\ \mu\text{m}$  diameter are produced via electron-beam lithography and plasma etching. The sample is planarized with benzocyclobutene, and individual micropillars are electrically contacted with circular gold contacts. The  $Q$  factor of the electrically contacted micropillars is about 20 000. Details on the sample fabrication are explained in Ref. [39].

The microlaser sample is placed in a continuous-flow He cryostat and cooled down to a temperature of  $T = 15\ \text{K}$  (see Fig. 1). It is pumped by an electrical pulse generator with a variable pulse length (0.5–10 ns) and a pulse amplitude of up to  $5.1\ V_{\text{ac bias}}$  and a repetition frequency of 10 kHz. A bias voltage  $V_{\text{bias}} = V_{\text{dc bias}} + V_{\text{ac bias}}$  with  $V_{\text{dc bias}} = 1.5\ \text{V}$  is applied. For laser A, a pulse length of  $\tau_p = 2\ \text{ns}$ —and for laser B a pulse length of  $\tau_p = 1.5\ \text{ns}$ —is chosen as the best balance between coherence time limitations and a sufficient pulse area to reach the lasing regime, respectively. A microscope objective collects the emission. Polarization optics are used to separate the two orthogonal modes, and their emission is spectrally resolved by a spectrometer with a resolution of  $30\ \mu\text{eV}$ . Finally, the signal is analyzed with a TES or, alternatively, by a HBT setup.

The TES acts as a highly sensitive calorimeter to detect the small energy input from an absorbed photon pulse. The temperature change is measured with a sensitive thermometer which is, simultaneously, the absorber. By voltage biasing, the TES heats up within the superconducting phase transition and is stabilized by negative electrothermal feedback [2] so that the absorption of a photon pulse results ultimately in a current redistribution. The current change is measured via an inductively coupled two-stage dc

superconducting quantum-interference device (SQUID) [40]. The TES-SQUID detector unit is fiber coupled and mounted on the cold stage of an adiabatic demagnetization refrigerator, which is stabilized at 130 mK. From analyzing many pulses, a histogram of the photon-number distribution can be extracted. The detection efficiency of the TES is determined to be 87% [41].

### IV. EXPERIMENTAL RESULTS

Owing to a slightly asymmetric cross section of the micropillar, the degeneracy of the fundamental emission mode is lifted [42] and two orthogonally polarized linear mode components with a splitting of  $20\ \mu\text{eV}$  are observed. Both fundamental mode components couple to the common gain medium and show lasing influenced by gain competition, while higher-order lateral modes have much less spectral overlap with the quantum-dot gain and do not show lasing [26]. The intensity-bias voltage dependence of laser A [Fig. 2(a)] reveals the typical behavior: At first, both modes increase superlinearly at the threshold, then, at higher excitation gain, competition leads to a further increase in the strong mode (the blue squares) [22].

Figures 2(b)–2(d) depict the photon-number distribution for three voltages. For low-voltage pulses, both modes have a Poissonian distribution. The microlaser is expected to emit thermal light, but since the coherence time is shorter than the

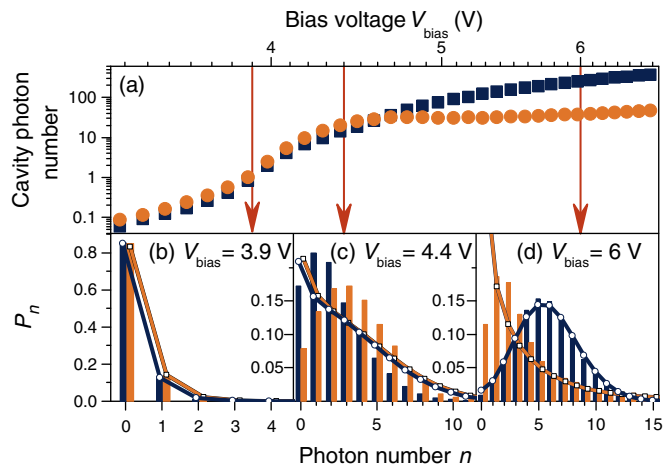


FIG. 2. (a) Intensity-bias voltage characteristic of laser A. The strong mode (the blue squares) shows an S-shaped behavior, while the weak mode (the orange circles) saturates in intensity (given as the number of photons inside the cavity, set to 1 at the laser threshold) above the threshold. (b)–(d) Photon statistics at three bias voltages, indicated by the red arrows. The bars correspond to the statistics measured with the TES; the dots, connected by a line, correspond to the theory. (b) For low bias voltage ( $V_{\text{bias}} = 3.9\ \text{V}$ ), both modes possess a Poissonian distribution. (c) Above threshold ( $V_{\text{bias}} = 4.4\ \text{V}$ ), the photon statistics exhibits a transient distribution which is partly thermal and partly Poissonian. (d) For high voltage ( $V_{\text{bias}} = 6.0\ \text{V}$ ), the weak mode shows a thermal distribution, whereas the strong mode exhibits a Poissonian distribution.

pulse length  $\tau_{\text{coh}} \ll \tau_p$ , the real character is not accessible in this regime since thermal bunching arises on a scale of the coherence time [26]. Therefore, a longer pulse averages over many bunching events and a Poissonian distribution is measured [43]. The coherence time at the bias voltage of 3.9 V can be estimated from the linewidth as  $\tau_{\text{coh}} \sim 170$  ps [44]. The theoretical calculations (dots connected by a line) which are detailed below do not suffer from coherence time limitations and reproduce a thermal distribution almost perfectly. For these low photon numbers, the two distributions are almost indistinguishable to the eye.

Above the threshold at  $V_{\text{bias}} = 4.4$  V, both modes are in a transient state and the photon-number distribution is partly thermal and partly Poissonian [45]. In this mixed photon-number distribution, the Poissonian part, which indicates the emission of coherent light, is recognizable by the enhanced contribution of higher photon numbers. Our theory describes the same behavior; however, without coherence time limitation, it predicts a higher probability for zero-photon events when compared to the experimental data.

For a high bias voltage of 6.0 V, the photon-number distribution for the weak and the strong mode differs considerably. Whereas the strong mode emits pure coherent light, indicated by Poissonian statistics, emission of the weak mode has thermal properties. The experimental photon-number distribution of the strong mode is in good agreement with theory. Since the coherence time ( $\tau_{\text{coh,w}} \sim 530$  ps) is shorter than the pulse length ( $\tau_p \sim 2$  ns), a pure thermal distribution cannot be measured for the weak mode. This observation explains again the deviation between theory and experiment noticeable at low photon numbers  $\leq 5$ .

Interestingly, while standard HBT measurements provide only information about the second-order autocorrelation function, all moments—and hence all orders—of the autocorrelation function at zero-time delay  $g^{(k)}(0)$  can be calculated from the experimentally determined photon-number distribution  $P_n$  [46]:

$$g^{(k)}(0) = \frac{\sum_n \prod_{i=0}^{k-1} (n-i) \cdot P_n}{\langle n \rangle^k}. \quad (1)$$

To determine the second-order autocorrelation function  $g^{(2)}(0)$ , only the mean photon number  $\langle n \rangle = \sum_n n P_n$  and the variance  $\mathcal{V}(n) = \langle (n - \langle n \rangle)^2 \rangle$  are required:

$$g^{(2)}(0) = 1 + \frac{\mathcal{V}(n) - \langle n \rangle}{\langle n \rangle^2}. \quad (2)$$

In Fig. 3(a), the  $g^{(2)}(0)$  values of laser A for varied pulse voltages are presented. The data calculated from the TES measurements are in close-to-perfect agreement with the corresponding HBT data. At low voltage, the thermal emission with an expected  $g^{(2)}(0) = 2$  is, as already discussed, not resolvable, and a  $g^{(2)}(0) = 1$  value is measured. In the transition region, an increase of up to

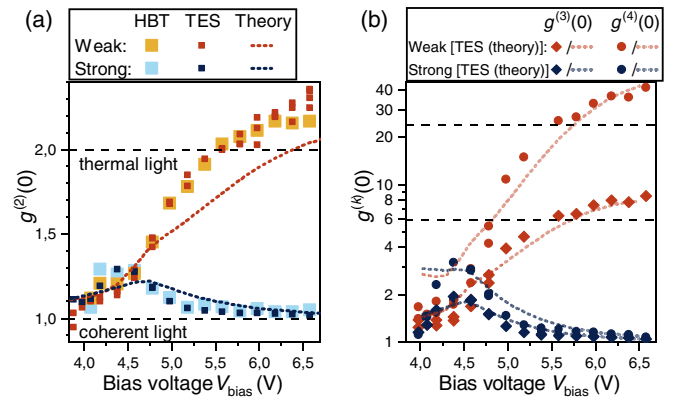


FIG. 3. Laser A. (a) The second-order autocorrelation function at zero-time delay  $g^{(2)}(0)$  determined by the TES (the small, darker symbols) is in very good agreement with the one determined by the HBT (the big, brighter symbols) and the theory (the dashed curves). The strong mode shows a transition from thermal to coherent emission. The weak mode increases in  $g^{(2)}(0)$  to values slightly above the thermal limit. The dashed lines indicate the respective thermal values  $k!$ . (b) The third and fourth orders of the autocorrelation function  $g^{(n)}(0)$  from the same TES measurements exhibit behavior analogous to that of  $g^{(2)}(0)$ .

1.3 is visible. This change represents the transition from thermal emission to lasing operation, with a simultaneous increase of the coherence time [25,26,47]. The autocorrelation of the strong mode decreases to  $g^{(2)}(0) = 1$  for higher voltage, indicating coherent emission. For the weak mode, the autocorrelation increases to values slightly above 2. This behavior, i.e.,  $g^{(2)}(0) > 2$ , is an indication for thermal emission with minor contributions from mode coupling [22]. The accordance of both techniques proves the accuracy of the determined  $g^{(2)}(0)$  value.

The third and fourth orders of the autocorrelation function [see Eq. (1)] obtained from the TES data are depicted in Fig. 3(b). The different orders of  $g^{(k)}(0)$  follow the same trend as  $g^{(2)}(0)$  but reach higher values, and the theoretical simulations confirm this behavior. Deviations between experimental and theoretical  $g^{(4)}(0)$  values at low bias voltages are attributed to additional temporal resolution limitations not considered in our theory. Being able to address higher-order photon autocorrelation functions to, e.g., better understand the threshold behavior of microlasers [48] is another advantage of the TES technique. Indeed, higher-order autocorrelations cannot be accessed by standard HBT experiments, and, to date, only elaborate streak-camera measurements have allowed us to access the autocorrelation function up to fourth order [49,50].

To highlight the importance of investigating microlasers with a TES, a second laser, B, with almost identical input-output and autocorrelation characteristics (see the insets of Fig. 4) is investigated. Analyzing its full photon statistics, accessible only with a TES, we see substantial differences between laser A and laser B. Compared to laser A, both the weak and the strong mode show a behavior with an

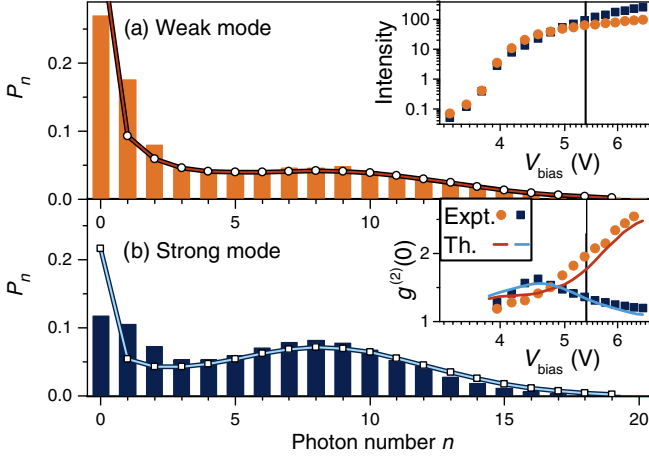


FIG. 4. Laser *B*. The photon-number distributions of the (a) weak mode and (b) strong mode at  $V_{\text{bias}} = 5.4$  V can best be described by an overlay of a thermal distribution with a low mean photon number  $\langle n \rangle$  and a Poissonian distribution with a high  $\langle n \rangle$  value. [Inset of (a)] The input-output characteristic and [inset of (b)]  $g^{(2)}(0)$  values of laser *B* are similar to laser *A* (cf. Figs. 2 and 3).

emission being composed of a thermal distribution with a low mean photon number  $\langle n \rangle$  and a Poissonian distribution with a large  $\langle n \rangle$  value. In striking contrast to the statistics of laser *A*, for laser *B*, the zero-photon state is the most likely one for both the strong and the weak mode. The difference between the weak and the strong mode results in the fact that the emission statistics of the former mode is dominated by the thermal part, whereas the strong mode is dominated by the Poissonian part. This behavior can be explained as follows: Both modes are potential lasing modes where carrier fluctuations largely influence the switch-on process. The photon statistics at  $V_{\text{bias}} = 5.4$  V are exemplary. This behavior can be observed for a wide excitation range.

For every electrical pulse, each of the two modes could potentially reach the lasing regime, while the other mode stays in the thermal regime. In the presented case, the analysis of the experimental photon-number distributions yields that, in about 75% of the pulses, the strong mode is in the lasing regime and emits coherent light, while the weak mode radiates thermally. In the other approximately 25% of the pulses, the weak mode is lasing and the strong mode is not. This bimodal behavior is comparable to spontaneous switching under continuous-wave excitation [22,27]. Simultaneously, the dwell time (the average time before a mode switch) is assumed to be large compared to the pulse length, but it is not accessible for pulsed excitation. Also, the theoretical description reproduces this behavior well in both the photon-number distribution and the  $g^{(2)}(0)$  values. In the master equation, the spontaneous transition between the modes is effectively reduced (compared to laser *A*) due to stronger modal interactions and carrier population oscillations [30], thus trapping the weak

mode close to the zero-photon state and giving rise to bistable behavior [36].

## V. CONCLUSION

We demonstrate in this paper that TESs are powerful detectors to investigate the photon statistics of microscopic laser devices. Where former HBT experiments were able only to detect intensity fluctuations quantified in  $g^{(2)}(0)$ , regardless of their origin, the TES gives direct access to the photon-number distribution and enables the differentiation between various effects. Determining the full photon statistics via TES detectors has great potential to become a powerful characterization method to reveal and understand the physics of nanophotonic devices at the quantum level [51]. It will be of particular importance for the further development of microcavities towards applications which benefit from a tunable and controllable photon statistics of emission.

## ACKNOWLEDGMENTS

The research leading to these results has received funding from the European Research Council under the European Union's Seventh Framework ERC Grant Agreement No. 615613, within the EURAMET joint research project MIQC2 from the European Union's Horizon 2020 Research and Innovation Programme and the EMPIR Participating States, and from the German Research Foundation under Projects No. RE2974/10-1 and No. Ka 2318/7-1. The authors thank the State of Bavaria for the financial support and A. E. Lita and S. W. Nam for providing the TES detector chips.

## APPENDIX: DETAILS OF THE THEORETICAL METHODS

To describe the measurement theoretically, we divide the process into two subprocesses: (i) the excitation of the laser device by the pump pulse and (ii) the subsequent detection of the emitted cavity photons. The first subprocess is modeled by the steady state of the master equation (A1), which is determined by solving the linear equation  $(d/dt)\rho_N^n = 0$  [see Eq. (A1)]. This steady state is then modified according to Ref. [38] [see Eq. (A2)].

### 1. Master equation

The utilized master equation

$$\begin{aligned} \frac{d}{dt}\rho_N^n &= P[\rho_{N-1}^n - \rho_N^n] - \tau^{-1}[N\rho_N^n - (N+1)\rho_{N+1}^n] \\ &\quad - \sum_i g_i [N(n_i+1)\rho_N^n - (N+1)n_i\rho_{N+1}^{n-e_i}] \\ &\quad - \sum_i \ell_i [n_i\rho_N^n - (n_i+1)\rho_N^{n+e_i}] - \sum_{i,j} R_{i \rightarrow j} [n_i(n_j+s)\rho_N^n \\ &\quad - (n_i+1)(n_j-1+s)\rho_N^{n+e_i-e_j}] \end{aligned} \quad (\text{A1})$$

TABLE I. Simulation parameters used in Figs. 2 and 4.

Parameter	Figure 2	Figure 4
$s$	0.6	1
In units of $\tau$ :		
$l_1$	0.1	0.1
$l_2$	0.105	0.105
$g_1$	0.14	0.14
$g_2$	0.12	0.12
$R_{21}$	0.03	0.03
$R_{12}$	0.00325	0.00325
In units of $P_{\text{thr}}$ :		
$P_b$	0.2	
$P_c$	1.6 (4.4 V)	
$P_d$	8.0 (6.0 V)	
$P$		2.9 (5.4 V)

is based on a phenomenological model that takes all of the relevant processes of the microcavity laser into account. Here,  $P$  is the pump rate,  $\tau^{-1}$  is the rate of spontaneous emission into nonlasing modes,  $g_i$  is the rate of emission into the lasing mode  $i$ ,  $\ell_i$  is the loss rate of photons from cavity  $i$ , and  $R_{i \rightarrow j}$  is the transition rate of the cavity photons from mode  $i$  to mode  $j$ .  $s$  is the factor quantifying how strong the gain-medium induced mode interaction effectively reduces the spontaneous emission between the modes. The solution of Eq. (A1) can be interpreted as the diagonal elements of the density matrix  $\langle \mathbf{n}, N | \rho | \mathbf{n}, N \rangle = \rho_{\mathbf{n}}^{\mathbf{n}}$ , giving the probability to find the system with  $N$  excited emitters and  $\mathbf{n} = (n_w, n_s)$  photons in the weak mode and strong mode, respectively. By tracing over the emitters and one of the modes, one can obtain, for example, the distribution of the weak mode  $P_{n_w} = \sum_{N, n_s} \rho_{\mathbf{n}}^{\mathbf{n}}$ . The parameters for the theory are given in Table I.

## 2. Detection model

Since the master equation models the inside of the cavity, it is necessary to study the change of the statistics with respect to the leakage of photons out of the cavity  $\ell_i$  and the nonideal setup, with an efficiency denoted by  $\xi$ . Assuming that the leakage of the cavity is the relevant process—i.e., the pump pulse has already subsided and the rate of the intermode kinetics is comparable small—the influence of the detection for a single-mode distribution can be modeled as

$$P_m^{\text{out}}(t_1, t_2) = \sum_{n_i=m} P_{n_i} \binom{n_i}{m} (1 - \xi e^{-\ell_i t_1} + \xi e^{-\ell_i t_2})^{n_i-m} \times (\xi e^{-\ell_i t_1} - \xi e^{-\ell_i t_2})^m, \quad (\text{A2})$$

where  $P_{n_i}$  is the single mode distribution [see Eq. (A1)],  $P_m^{\text{out}}$  is the detected distribution, and  $t_1$  and  $t_2$  are the times at which the measurement begins and ends, respectively

[38]. Although this transformation shifts the whole statistics to a lower mean number, it does not alter the photon autocorrelation  $g^{(2)}(0)$ . To prove this statement, we define  $\zeta = \xi e^{-\ell_i t_1} - \xi e^{-\ell_i t_2}$  and find that  $\langle n \rangle_{\text{out}}$  and  $\langle n^2 \rangle_{\text{out}}$  can be expressed by  $\zeta$  and the expectation values inside the cavity by

$$\begin{aligned} \langle n \rangle_{\text{out}} &= \zeta \langle n \rangle, \\ \langle n^2 \rangle_{\text{out}} &= \zeta^2 \langle n^2 \rangle + (\zeta - \zeta^2) \langle n \rangle. \end{aligned} \quad (\text{A3})$$

This follows from Eq. (A2) by changing the order of summation and using the knowledge of the mean and the variance of the binomial distribution.

Relations (A3) can be inserted into Eq. (2) and it follows that the transformation  $P_m^{\text{out}}(t_1, t_2)$  does not change  $g^{(2)}(0)$ . The setup efficiency is estimated to be  $\xi = 0.1$ . Since the measurement lasts much longer than the cavity decay time, we set  $t_2 \rightarrow \infty$  and  $t_1 = 0$  since the initial state for the detection model is the steady state of Eq. (A1).

- 
- [1] R. Hanbury-Brown and R. Q. Twiss, Correlation between photons in two coherent beams of light, *Nature (London)* **177**, 27 (1956).
  - [2] A. E. Lita, A. J. Miller, and S. W. Nam, Counting near-infrared single-photons with 95% efficiency, *Opt. Express* **16**, 3032 (2008).
  - [3] B. Cabrera, R. M. Clarke, P. Colling, A. J. Miller, S. W. Nam, and R. W. Romani, Detection of single infrared, optical, and ultraviolet photons using superconducting transition edge sensors, *Appl. Phys. Lett.* **73**, 735 (1998).
  - [4] K. D. Irwin and G. C. Hilton, Transition-edge sensors, in *Cryogenic Particle Detection*, edited by Ch. Enss, Topics in Applied Physics, Vol. 99 (Springer, New York, 2005), p. 63.
  - [5] A. J. Miller, S. W. Nam, J. M. Martinis, and A. V. Sergienko, Demonstration of a low-noise near-infrared photon counter with multiphoton discrimination, *Appl. Phys. Lett.* **83**, 791 (2003).
  - [6] A. Gatti, E. Brambilla, M. Bache, and L. A. Lugiato, Ghost Imaging with Thermal Light: Comparing Entanglement and Classical Correlation, *Phys. Rev. Lett.* **93**, 093602 (2004).
  - [7] D.-Z. Cao, G.-J. Ge, and K. Wang, Two-photon subwavelength lithography with thermal light, *Appl. Phys. Lett.* **97**, 051105 (2010).
  - [8] F. Boitier, A. Godard, E. Rosencher, and C. Fabre, Measuring photon bunching at ultrashort timescale by two-photon absorption in semiconductors, *Nat. Phys.* **5**, 267 (2009).
  - [9] W. Denk, J. H. Strickler, and W. W. Webb, Two-photon laser scanning fluorescence microscopy, *Science* **248**, 73 (1990).
  - [10] A. Jechow, M. Seefeldt, H. Kurzke, A. Heuer, and R. Menzel, Enhanced two-photon excited fluorescence from imaging agents using true thermal light, *Nat. Photonics* **7**, 973 (2013).
  - [11] M. M-Tehrani and L. Mandel, Intensity fluctuations in a two-mode ring laser, *Phys. Rev. A* **17**, 694 (1978).

- [12] J. B. Khurgin and G. Sun, How small can “nano” be in a “nanolaser”?, *Nanophotonics* **1**, 3 (2012).
- [13] S. Kreinberg, T. Grbešić, M. Strauß, A. Carmele, M. Emmerling, C. Schneider, S. Höfling, X. Porte, and S. Reitzenstein, Quantum-optical spectroscopy of a two-level system using an electrically driven micropillar laser as resonant excitation source, *Light Sci. Appl.* (to be published).
- [14] M. Nomura, N. Kumagai, S. Iwamoto, Y. Ota, and Y. Arakawa, Laser oscillation in a strongly coupled single-quantum-dot-nanocavity system, *Nat. Phys.* **6**, 279 (2010).
- [15] R. F. Oulton, V. J. Sorger, T. Zentgraf, R.-M. Ma, C. Gladden, L. Dai, G. Bartal, and X. Zhang, Plasmon lasers at deep subwavelength scale, *Nature (London)* **461**, 629 (2009).
- [16] S. Reitzenstein, A. Bazhenov, A. Gorbunov, C. Hofmann, S. Münch, A. Löffler, M. Kamp, J. P. Reithmaier, V. D. Kulakovskii, and A. Forchel, Lasing in high- $Q$  quantum-dot micropillar cavities, *Appl. Phys. Lett.* **89**, 051107 (2006).
- [17] M. Lermer, N. Gregersen, M. Lorke, E. Schild, P. Gold, J. Mørk, C. Schneider, A. Forchel, S. Reitzenstein, S. Höfling, and M. Kamp, High beta lasing in micropillar cavities with adiabatic layer design, *Appl. Phys. Lett.* **102**, 052114 (2013).
- [18] G. Björk, A. Karlsson, and Y. Yamamoto, Definition of a laser threshold, *Phys. Rev. A* **50**, 1675 (1994).
- [19] S. Kreinberg, W. W. Chow, J. Wolters, C. Schneider, C. Gies, F. Jahnke, S. Höfling, M. Kamp, and S. Reitzenstein, Emission from quantum-dot high-beta microcavities: Transition from spontaneous emission to lasing and the effects of superradiant emitter coupling, *Light Sci. Appl.* **6**, e17030 (2017).
- [20] A. E. Siegman, *Lasers* (University Science Books, Sausalito, CA, 1986).
- [21] P. R. Rice and H. J. Carmichael, Photon statistics of a cavity-QED laser: A comment on the laser-phase-transition analogy, *Phys. Rev. A* **50**, 4318 (1994).
- [22] H. A. M. Leymann, C. Hopfmann, F. Albert, A. Foerster, M. Khanbekyan, C. Schneider, S. Höfling, A. Forchel, M. Kamp, J. Wiersig, and S. Reitzenstein, Intensity fluctuations in bimodal micropillar lasers enhanced by quantum-dot gain competition, *Phys. Rev. A* **87**, 053819 (2013).
- [23] E. Schlottmann, S. Holzinger, B. Lingnau, K. Lüdge, C. Schneider, M. Kamp, S. Höfling, J. Wolters, and S. Reitzenstein, Injection Locking of Quantum-Dot Microlasers Operating in the Few-Photon Regime, *Phys. Rev. Applied* **6**, 044023 (2016).
- [24] F. Jahnke, C. Gies, M. Aßmann, M. Bayer, H. A. M. Leymann, A. Foerster, J. Wiersig, C. Schneider, M. Kamp, and S. Höfling, Giant photon bunching, superradiant pulse emission and excitation trapping in quantum-dot nanolasers, *Nat. Commun.* **7**, 11540 (2016).
- [25] S. T. Jagsch, N. V. Triviño, F. Lohof, G. Callsen, S. Kalinowski, I. M. Rousseau, R. Barzel, J.-F. Carlin, F. Jahnke, R. Butte, C. Gies, A. Hoffmann, N. Grandjean, and S. Reitzenstein, A quantum optical study of thresholdless lasing features in high- $\beta$  nitride nanobeam cavities, *Nat. Commun.* **9**, 564 (2018).
- [26] S. M. Ulrich, C. Gies, S. Ates, J. Wiersig, S. Reitzenstein, C. Hofmann, A. Löffler, A. Forchel, F. Jahnke, and P. Michler, Photon Statistics of Semiconductor Microcavity Lasers, *Phys. Rev. Lett.* **98**, 043906 (2007).
- [27] C. Redlich, B. Lingnau, S. Holzinger, E. Schlottmann, S. Kreinberg, C. Schneider, M. Kamp, S. Höfling, J. Wolters, S. Reitzenstein, and K. Lüdge, Mode-switching induced super-thermal bunching in quantum-dot microlasers, *New J. Phys.* **18**, 063011 (2016).
- [28] M. Fanaei, A. Foerster, H. A. M. Leymann, and J. Wiersig, Effect of direct dissipative coupling of two competing modes on intensity fluctuations in a quantum-dot-microcavity laser, *Phys. Rev. A* **94**, 043814 (2016).
- [29] M. M-Tehrani and L. Mandel, Coherence theory of the ring laser, *Phys. Rev. A* **17**, 677 (1978).
- [30] M. Marconi, J. Javaloyes, F. Raineri, J. A. Levenson, and A. M. Yacomotti, Asymmetric mode scattering in strongly coupled photonic crystal nanolasers, *Opt. Lett.* **41**, 5628 (2016).
- [31] B. L. Zhelnov, V. S. Smirnov, and A. P. Fadeev, The instability of unidirectional radiation in a ring laser, *Opt. Spectrosc.* **28**, 400 (1970).
- [32] L. Mandel and E. Wolf, *Optical Coherence and Quantum Optics* (Cambridge University Press, Cambridge, England, 1995).
- [33] M. O. Scully and W. E. Lamb, Jr., Quantum theory of an optical maser. I. General theory, *Phys. Rev.* **159**, 208 (1967).
- [34] C. Gies, J. Wiersig, M. Lorke, and F. Jahnke, Semiconductor model for quantum-dot-based microcavity lasers, *Phys. Rev. A* **75**, 013803 (2007).
- [35] D. Vorberg, W. Wustmann, R. Ketzmerick, and A. Eckardt, Generalized Bose-Einstein Condensation into Multiple States in Driven-Dissipative Systems, *Phys. Rev. Lett.* **111**, 240405 (2013).
- [36] H. A. M. Leymann, D. Vorberg, T. Lettau, C. Hopfmann, C. Schneider, M. Kamp, S. Höfling, R. Ketzmerick, J. Wiersig, S. Reitzenstein, and A. Eckardt, Pump-Power-Driven Mode Switching in a Microcavity Device and Its Relation to Bose-Einstein Condensation, *Phys. Rev. X* **7**, 021045 (2017).
- [37] M. Khanbekyan, H. A. M. Leymann, C. Hopfmann, A. Foerster, C. Schneider, S. Höfling, M. Kamp, J. Wiersig, and S. Reitzenstein, Unconventional collective normal-mode coupling in quantum-dot-based bimodal microlasers, *Phys. Rev. A* **91**, 043840 (2015).
- [38] C. T. Lee, External photodetection of cavity radiation, *Phys. Rev. A* **48**, 2285 (1993).
- [39] C. Böckler, S. Reitzenstein, C. Kistner, R. Debusmann, A. Löffler, T. Kida, S. Höfling, A. Forchel, L. Grenouillet, J. Claudon, and J. M. Gérard, Electrically driven high- $Q$  quantum dot-micropillar cavities, *Appl. Phys. Lett.* **92**, 091107 (2008).
- [40] D. Drung, C. Abmann, J. Beyer, A. Kirste, M. Peters, F. Ruede, and T. Schurig, Highly sensitive and easy-to-use SQUID sensors, *IEEE Trans. Appl. Supercond.* **17**, 699 (2007).
- [41] M. Schmidt, M. v. Helversen, M. López, F. Gericke, E. Schlottmann, T. Heindel, S. Kück, S. Reitzenstein, and J. Beyer, Photon-number-resolving transition-edge sensors for the metrology of quantum light sources, *J. Low Temp. Phys.*, DOI: 10.1007/s10909-018-1932-1 (2018).

- [42] S. Reitzenstein, C. Hofmann, A. Gorbunov, M. Strauß, S. H. Kwon, C. Schneider, A. Löffler, S. Höfling, M. Kamp, and A. Forchel, AlAs/GaAs micropillar cavities with quality factors exceeding 150.000, *Appl. Phys. Lett.* **90**, 251109 (2007).
- [43] R. Loudon, *The Quantum Theory of Light*, 2nd ed. (Oxford University Press, New York, 1983).
- [44] S. Ates, S. M. Ulrich, P. Michler, S. Reitzenstein, A. Löffler, and A. Forchel, Coherence properties of high-beta elliptical semiconductor micropillar lasers, *Appl. Phys. Lett.* **90**, 161111 (2007).
- [45] F. Arecchi, A. Berne, A. Sona, and P. Burlamacchi, Photon-count distributions and field statistics, *IEEE J. Quantum Electron.* **2**, 341 (1966).
- [46] M. J. Stevens, Photon statistics, measurements, and measurements tools, in *Single-Photon Generation and Detection: Physics and Applications*, edited by Alan Migdall, Sergey V. Polyakov, Jingyun Fan, and Joshua C. Bienfang, Vol. 45 (Academic Press, New York, 2013), p. 25.
- [47] S. Strauf, K. Hennessy, M. Rakher, Y.-S. Choi, A. Badolato, L. Andreani, E. Hu, P. Petroff, and D. Bouwmeester, Self-Tuned Quantum Dot Gain in Photonic Crystal Lasers, *Phys. Rev. Lett.* **96**, 127404 (2006).
- [48] H. A. M. Leymann, A. Foerster, and J. Wiersig, Expectation value based equation-of-motion approach for open quantum systems: A general formalism, *Phys. Rev. B* **89**, 085308 (2014).
- [49] M. Aßmann, F. Veit, M. Bayer, M. van der Poel, and J. M. Hvam, Higher-order photon bunching in a semiconductor microcavity, *Science* **325**, 297 (2009).
- [50] J. Wiersig, C. Gies, F. Jahnke, M. Aßmann, T. Berstermann, M. Bayer, C. Kistner, S. Reitzenstein, C. Schneider, S. Höfling, A. Forchel, C. Kruse, J. Kalden, and D. Hommel, Direct observation of correlations between individual photon emission events of a microcavity laser, *Nature (London)* **460**, 245 (2009).
- [51] M. Klaas, E. Schlottmann, H. Flayac, F.P. Laussy, F. Gericke, M. Schmidt, M. v. Helversen, J. Beyer, S. Brodbeck, H. Suchomel, S. Höfling, S. Reitzenstein, and C. Schneider, Photon Number-Resolved Measurement of an Exciton-Polariton Condensate, [arXiv:1805.02959](https://arxiv.org/abs/1805.02959) [*Phys. Rev. Lett.* (to be published)].